Research Square

Preprints are preliminary reports that have not undergone peer review.
They should not be considered conclusive, used to inform clinical practice,
or referenced by the media as validated information.

Clinical Application of a Dual-Threshold Bolus Tracking Protocol in One-Stop Combined CT Angiography and Venography of the Lower Extremities: A Prospective Comparative Observational Study

Qing-Peng Zhan
The First Affiliated Hospital of Jinan University
Shang-Ao Gong
The First Affiliated Hospital of Jinan University
Yu-Long Xie
The First Affiliated Hospital of Jinan University
Ting Wang
The First Affiliated Hospital of Jinan University
Hao Zhou
The First Affiliated Hospital of Jinan University
Chang-Zheng Shi
tsczcn@jnu.edu.cn

The First Affiliated Hospital of Jinan University

Research Article

Keywords: Lower extremity CT angiography, Lower extremity CT venography, Dual-threshold bolus tracking, Individualized scanning

Posted Date: July 14th, 2026

DOI: https://doi.org/10.21203/rs.3.rs-10155544/v1

License: This work is licensed under a Creative Commons Attribution 4.0 International License.
Read Full License

Additional Declarations: No competing interests reported.

Abstract

Background

To compare the image quality of a personalized dual-threshold bolus tracking technique in one-stop combined lower extremity computed tomography angiography and venography (CTA-CTV).

Materials and Methods

Sixty-eight patients with suspected lower extremity vascular disease were enrolled and randomly divided into a control group (fixed delay, n = 34) and an experimental group (dual-threshold tracking, n = 34). All subjects underwent CT scanning using a 256-slice CT scanner. The experimental group employed a real-time triggering technique with monitoring points at the distal abdominal aorta and the popliteal vein, enabling individualized scan initiation in response to real-time venous opacification. The control group utilized a fixed 165-second delay for venous phase acquisition. Image quality was evaluated both objectively (quantitative parameters) and subjectively by two radiologists using a 4-point scale. This study was designed as a comparative imaging technique evaluation rather than a therapeutic intervention.

Results

Baseline characteristics and arterial phase quality did not differ significantly between groups ($P > 0.05$). However, the experimental group demonstrated significantly higher objective image quality parameters in the venous segments. Marked differences were observed in mean CT attenuation (156.9 ± 17.6 vs. 122.0 ± 11.1 HU) and CNR (11.5 ± 2.5 vs. 7.1 ± 1.7) of the popliteal vein ($P < 0.001$). The proportion of diagnostic-quality venous images (score ≥ 3) was significantly higher in the experimental group than in the control group (88.2% vs. 55.9%, $P < 0.001$).

Conclusions

By monitoring real-time venous filling, this personalized dual-threshold bolus tracking protocol effectively accommodates individual hemodynamic differences, resulting in significantly superior venous image quality in one-stop lower extremity CTA-CTV, while maintaining arterial enhancement and radiation dose at conventional levels.

Trial registration:

Not applicable (non-interventional comparative imaging technique evaluation).

Background

The aging global population is driving an increasing incidence of peripheral vascular disease (PVD), posing a significant public health challenge. Peripheral arterial disease (PAD), a major subtype of PVD, is becoming increasingly prevalent worldwide. Recent data indicate that global PAD cases reached 113 million in 2021 and are projected to surge to 363 million by 2050—an increase of 220% [1]. Patients with PAD face substantial risks of disease progression; a MarketScan database study revealed that approximately 11.08% of these patients develop chronic limb ischemia (CLI) annually [2]. Given the high morbidity and mortality associated with this condition, early, precise identification and intervention are essential to halt disease progression [3–5]. However, lower extremity vascular disease often presents insidiously with non-specific symptoms; only 10%–30% of patients present with classic manifestations such as intermittent claudication [6]. Current screening methods, including the ankle-brachial index (ABI) and exercise stress testing, face limitations. For instance, vascular medial calcification often falsely elevates ABI values, failing to accurately reflect the true severity of stenosis. Similarly, comorbid cardiopulmonary insufficiency or osteoarticular disease frequently complicates exercise stress testing, which hinders early diagnosis [7]. Furthermore, as lower extremity arteriosclerosis is often comorbid with venous thromboembolic disease [8], combined assessment of both the arterial and venous systems is essential.

Non-invasive imaging modalities demonstrate high reproducibility and have become the cornerstone of vascular assessment. Common modalities include Magnetic Resonance Imaging (MRI), Ultrasonography (US), Digital Subtraction Angiography (DSA), and Computed Tomography Angiography (CTA). However, each has drawbacks. MRI requires long scan times and has limited sensitivity in detecting calcified plaques [9]. US is operator-dependent and often limited by anatomy [10] and the accuracy of diagnostic relies on doctor’s expertise [11]. Digital subtraction angiography (DSA) remains the reference standard for evaluating peripheral arterial disease; however, its routine clinical utility is limited by its invasiveness, procedural risks, and reliance on ionizing radiation [12]. Computed tomography angiography (CTA) has become the preferred method for evaluating lower extremity vasculature due to its speed, non-invasiveness, and superior three-dimensional visualization [13]. Performing separate scans for CTA and CTV would significantly increase radiation dose, which violates the ALARA (As Low As Reasonably Achievable) principle [14], while also increasing contrast burden and necessitating a second puncture, thereby limiting its clinical feasibility. Therefore, a one-stop imaging approach for the lower extremity arteriovenous system is of significant clinical importance. Nevertheless, current one-stop imaging of the lower extremity arteriovenous system remains limited: traditional one-stop lower extremity arteriovenous CT angiography protocols typically rely on fixed or empirical scan delays, which cannot reliably accommodate individual hemodynamic variations caused by differences in cardiac function or vascular obstruction severity. This often leads to suboptimal capture of the arterial or venous phase, thereby compromising diagnostic accuracy [15] .

To overcome the limitations of current one-stop lower extremity arteriovenous imaging, this study proposes a personalized CT scanning protocol based on dual-threshold bolus tracking. Specifically, we selected the distal abdominal aorta and popliteal vein as monitoring points [16, 17] and assigned specific attenuation thresholds to each site (artery: 150 HU; vein: 120 HU) to construct this "dual-threshold"

triggering strategy. This prospective comparative observational imaging study aims to assess the feasibility and clinical utility of this individualized protocol in overcoming hemodynamic variations and optimizing image quality.

Methods

(1) Study Population

This prospective comparative imaging study consecutively enrolled patients with suspected lower extremity vascular disease undergoing CTA-CTV at the First Affiliated Hospital of Jinan University from May 2024 to May 2025. A total of 68 participants were enrolled based on predefined inclusion and exclusion criteria. Ethical approval was granted by the Ethics Committee of the First Affiliated Hospital of Jinan University (Approval No. KY-2024-151), and written informed consent was obtained from all participants.

Inclusion criteria:

(1) Patients with suspected lower extremity vascular disease scheduled for CTA/CTV due to symptoms (e.g., pain, claudication, swelling) and/or an abnormal ankle-brachial index (ABI < 0.9);

(2) Age ≥ 18 years;

(3) Conscious and cooperative, and able to provide written informed consent;

(4) No contraindications to the use of iodinated contrast media;

Exclusion criteria:

(1) Severe renal insufficiency (estimated glomerular filtration rate [eGFR] < 30 mL/min/1.73 m²) or severe cardiac insufficiency (New York Heart Association [NYHA] Class ≥ IV) [18] ;

(2) Known hypersensitivity to iodinated contrast media;

(3) Presence of internal/external fixation implants in the lower extremities or a history of amputation;

(4) Pregnancy or lactation;

Sample Size, Randomization, and Blinding

Based on preliminary data (effect size = 0.8), with a significance level of 0.05 and a power of 0.90, a minimum sample size of 34 patients per group was required. Sixty-eight participants were randomly assigned to the experimental group or the control group in a 1:1 ratio. The random allocation sequence was generated by a statistician not involved in patient recruitment, using SPSS 26.0. A research nurse

enrolled participants and opened sequentially numbered, opaque, sealed envelopes to assign them to groups. CT technologists were blinded to group assignment until the examination began.

Equipment and Image Acquisition Protocols

Equipment and Contrast Administration

All examinations were performed on a 256-slice wide-detector CT scanner (NeuViz Epoch; Neusoft Medical Systems, Shenyang, China). The contrast medium iopromide (Ultravist 370; Bayer Healthcare, Berlin, Germany) was administered using a dual-head power injector (Nemoto; Nemoto Kyorindo Co., Ltd., Tokyo, Japan). Image analysis was performed on an AVW workstation (Neusoft Medical Systems, Shenyang, China).

Scanning Parameters

Participants were positioned supine, feet-first, with the arms extended above the head. The scan range extended from the lower margin of the L3 vertebra to the soles of the feet.

Arterial phase parameters: 100 kV tube voltage; automatic tube current modulation (ATCM) at a reference tube current of 150 mAs; 0.5 s rotation time; pitch 0.8; collimation 128 × 0.625 mm; matrix 512 × 512. All images were reconstructed using an iterative reconstruction algorithm (F20) with a window width of 400 HU and window level of 80 HU. Venous phase parameters: 80 kV tube voltage; ATCM with a reference tube current of 200 mAs; all other parameters were identical to those of the arterial phase.

Contrast Injection and Triggering Protocol

A 20-gauge intravenous catheter was placed in the right antecubital vein for a dual-phase injection protocol. Syringe A contained 95 mL of iopromide (Ultravist 370), and Syringe B contained 30 mL of normal saline. The injection sequence was as follows: 60 mL of contrast at 4.0 mL/s, followed by 35 mL of contrast at 2.5 mL/s, and finally a 30 mL normal saline flush at 2.5 mL/s. Consistent with prior studies [19, 20], the initial high flow rate was used to ensure rapid arterial enhancement, while the subsequent lower rate maintained a plateau of venous contrast concentration, thereby optimizing dual-phase imaging.

Experimental Group (Dual-Threshold Tracking):

Arterial Phase: A monitoring region of interest (ROI 1) was placed 2 cm above the distal bifurcation of the abdominal aorta (Tracker 1). Twelve seconds after injection, monitoring began. When the CT attenuation reached 150 HU in ROI 1, an 8-second delay was applied to trigger the craniocaudal scan. These thresholds (150 HU for the artery and 120 HU for the vein) were determined based on our institutional pilot study and previous literature [19, 21] .

Venous Phase: A second monitoring ROI (ROI 2) was placed at the popliteal vein level (Tracker 2). Monitoring began 90 seconds after injection and was conducted every three seconds thereafter. Upon reaching 120 HU threshold, the caudocranial venous scan in ROI 2 was initiated. In our pilot experiments, 120 HU was determined as the minimum attenuation required for adequate venous opacification, while a 90-second delay was implemented to avoid interference from residual arterial enhancement.

(2) Control Group (Fixed Delay): Arterial phase triggering was identical to that in the experimental group (Tracker 1, 150 HU threshold, 8-second scan delay). In the venous phase, a fixed delay mode was used: the scan was triggered 165 seconds after injection (caudocranial direction). The delay was determined by our routine protocol and the average peak time reported in the literature for venous vessels [15] .

The workflow is illustrated in Fig. 1.

Image Post-processing and Analysis

Image Processing

Raw data were transferred to the AVW workstation for the reconstruction of 1-mm thin-slice axial images. Secondary reformatted images—including multiplanar reconstruction (MPR), maximum intensity projection (MIP), and volume rendering (VR)—were subsequently generated for both arterial and venous phases. All DICOM datasets were archived within the Picture Archiving and Communication System (PACS).

Image Analysis and Evaluation

The VR, MIP, and axial images were independently assessed by two senior radiologists (with 12 and 15 years of experience in vascular imaging, respectively). The readers were blinded to patient data and scanning protocols. Prior to formal evaluation, the readers assessed a pilot set of images to calibrate scoring criteria. Any discrepancies were resolved by consensus.

Arterial Image Quality (4-point scale):

Score 1 (Poor): Very low attenuation, unclear margins, no distal branch visualization; non-diagnostic;

Score 2 (Fair): Low attenuation, blurred margins in some regions, partially unclear distal branches; limited diagnostic confidence;

Score 3 (Good/Diagnostic): Mildly decreased attenuation, mostly clear margins, adequate visualization of distal branches; diagnostic;

Score 4 (Excellent): High vessel attenuation, sharp vessel margins on VR/MIP, clear visualization of distal branches;

Venous Image Quality (4-point scale):

Score 1

Poor enhancement, unclear lumen; non-diagnostic;

Score 2

Inhomogeneous or weak enhancement, blurred segments; limited diagnostic confidence;

Score 3

Moderately homogeneous enhancement, clear lumen; diagnostic;

Score 4

Intense and homogeneous enhancement, clear lumen, no artifacts;

(2) Objective Evaluation

ROIs were placed on 1-mm axial images by an experienced radiologist, who measured each CT attenuation twice and averaged the results.

Vessel Attenuation (HU)

Arterial ROIs were placed in the distal abdominal aorta and in the common iliac, femoral, popliteal, and anterior tibial arteries. Venous ROIs were placed in the common iliac, external iliac, femoral, great saphenous, and popliteal veins.

ROI Placement

ROIs were placed at consistent anatomical levels, covering the full vessel cross-section while carefully avoiding calcifications, plaques, or focal stenosis.

Image Noise Measurement

For background noise measurement, an ROI was placed in a large homogeneous area of skeletal muscle on the ipsilateral limb at the same axial level as the target vascular ROI (e.g., the vastus intermedius at the mid-thigh or the gastrocnemius at the calf). The ROI was carefully positioned within the muscle parenchyma, avoiding intermuscular fat planes, fascia, and visible vessels. The muscle ROI area was kept nearly identical to that of the corresponding vascular ROI. The standard deviation (SD) of CT attenuation within the muscle ROI was recorded as image noise.

Calculations:

Signal-to-Noise Ratio (SNR) and Contrast-to-Noise Ratio (CNR) were calculated using the following formulas:

$$SNR = \frac{HU_{vessel}}{SD_{muscle}}$$

$$CNR = \frac{HU_{vessel} - HU_{muscle}}{SD_{muscle}}$$

Where HU_{vessel} is the CT attenuation of the vessel, HU_{muscle} is the CT attenuation of the muscle at the same level, and SD_{muscle} is the standard deviation of the muscle CT attenuation, representing image noise.

Radiation Dose Assessment

The dose-length product (DLP) and effective dose (ED) were recorded. ED was calculated as: $\mathrm{ED} = DLP \times k$, where k = 0.014 mSv·mGy⁻¹·cm⁻¹ [22] .

Statistical Analysis

All statistical analyses were performed using SPSS software (version 26.0; IBM Corp., Armonk, NY, USA). Categorical variables were expressed as frequencies and percentages (n [%]). Continuous variables were presented as mean $\pm$ standard deviation (SD). The Pearson χ^2 test (or Fisher's exact test when expected frequencies were < 5) was used to compare sex distribution. Continuous variables (age, BMI, CT attenuation, SNR, CNR, DLP, ED) were assessed for normality using the Shapiro-Wilk test and for homogeneity of variance using Levene's test. Normally distributed variables were compared using the independent samples t-test; otherwise, the Mann-Whitney U test was applied. Subjective image quality scores were compared using the Mann-Whitney U test. Inter-observer agreement was assessed using Cohen's kappa coefficient ($\kappa \geq 0.75$: excellent; $0.40 \leq \kappa < 0.75$: fair to acceptable; $\kappa < 0.40$: poor). A two-tailed P value < 0.05 was considered statistically significant. All analyses included all 68 allocated participants; no data were missing. No post-hoc analyses were performed.

Results

Baseline Characteristics of the Study Population

Between May 2024 and May 2025, 68 participants were enrolled and randomly assigned to the experimental group (n = 34) or the control group (n = 34) (Fig. 2). All 68 participants received their allocated scan protocol as intended with no losses to follow-up, and no concomitant treatments relevant to imaging outcomes were administered. No contrast-related adverse events (e.g., extravasation, allergic reactions) occurred in either group. Table 1 summarizes the baseline characteristics of the study population. There were no significant differences between the experimental and control groups in mean age (67.09 ± 12.73 vs. 69.97 ± 10.98 years), sex distribution, or body mass index (23.12 ± 2.96 vs. 23.96 ± 2.80 kg/m²) (all P > 0.05), indicating good between-group balance.

Table 1
Baseline Characteristics of the Study Population

Parameter	Control Group (n = 34)	Experimental Group (n = 34)	Statistic	*P*
Sex			$\chi^2 = 0.059$	0.808
Male	19(55.88%)	18(52.94%)		
Female	15(44.12%)	16(47.06%)		
Age (years)	69.97 ± 10.98	67.09 ± 12.73	*t* = 1.000	0.321
Height (m)	1.67 ± 0.06	1.68 ± 0.06	*t*=-0.371	0.712
Weight (kg)	66.79 ± 8.66	64.88 ± 8.97	*t* = 0.894	0.374
BMI (kg/m²)	23.96 ± 2.80	23.12 ± 2.96	*t* = 1.204	0.233

Note: Data are presented as mean ± standard deviation (SD) or n (%). BMI, body mass index.

Objective Evaluation

All objective image quality parameters (CT attenuation, SNR, and CNR) were normally distributed according to the Shapiro-Wilk test (all $P > 0.05$; see Supplementary Table S1). Data were expressed as mean ± SD, and between-group comparisons were performed using the independent samples *t*-test.

Arterial System

There were no statistically significant differences in CT attenuation, SNR, or CNR across any of the measured arterial segments between the two groups (all $P > 0.05$; Table S2).

Venous System

Across all measured venous segments—common iliac, external iliac, femoral, popliteal, and great saphenous veins—CT attenuation, SNR, and CNR were significantly higher in the experimental group than in the control group (all $P < 0.001$; Table 2).

Table 2
Objective Evaluation of Venous Imaging

Measurement Site	Parameter	Control Group	Experimental Group	*t*	*P*
Common iliac vein	CT attenuation (HU)	123.35 ± 12.84	159.96 ± 16.81	-10.090	< 0.001
	SNR	11.10 ± 1.18	15.21 ± 1.70	-11.568	< 0.001
	CNR	6.11 ± 1.16	9.74 ± 1.87	-9.614	< 0.001
External iliac vein	CT attenuation (HU)	125.43 ± 15.77	162.05 ± 17.82	-8.973	< 0.001
	SNR	11.14 ± 1.42	15.48 ± 1.82	-10.963	< 0.001
	CNR	6.12 ± 1.17	9.86 ± 1.95	-9.559	< 0.001
Femoral vein	CT attenuation (HU)	123.01 ± 13.21	158.11 ± 20.47	-8.400	< 0.001
	SNR	11.18 ± 1.18	15.46 ± 2.05	-10.561	< 0.001
	CNR	6.05 ± 1.25	10.03 ± 2.08	-9.584	< 0.001
Popliteal vein	CT attenuation (HU)	122.02 ± 11.12	156.88 ± 17.58	-9.774	< 0.001
	SNR	13.33 ± 1.48	18.37 ± 2.25	-10.923	< 0.001
	CNR	7.05 ± 1.70	11.54 ± 2.46	-8.751	< 0.001
Great saphenous vein	CT attenuation (HU)	122.95 ± 12.10	155.64 ± 25.10	-6.841	< 0.001
	SNR	12.96 ± 1.47	18.26 ± 2.72	-9.998	< 0.001
	CNR	7.11 ± 1.27	11.42 ± 2.96	-7.794	< 0.001

Note: SNR, signal-to-noise ratio; CNR, contrast-to-noise ratio; CT, computerized tomography.

Subjective Evaluation

Arterial System: Subjective image quality scores for the arterial system showed no statistically significant difference between the two groups ($Z = -0.136$, $P = 0.892$). Inter-observer agreement was excellent for both groups (control: $\kappa = 0.849$; experimental: $\kappa = 0.752$) (Table S3).

Venous System: Subjective image quality scores in the experimental group were significantly superior to those in the control group ($Z = -3.429$, $P < 0.001$). The proportion of diagnostic-quality images (score ≥ 3) was 88.2% (30/34) in the experimental group, which was significantly higher than the 55.9% (19/34) in the control group ($P < 0.001$). Inter-observer agreement was excellent for both groups (control: $\kappa = 0.951$; experimental: $\kappa = 0.950$) (Table 3).

Table 3
Subjective Evaluation of Venous Imaging

Group	Score 4	Score 3	Score 2	Score 1	Total	*Z*	*P*	*κ*
Control Group	4(11.76%)	15(44.12%)	15(44.12%)	0	34	-3.429	< 0.001	0.951
Experimental Group	14(41.18%)	16(47.06%)	4(11.76%)	0	34			0.950

Note: Data are presented as n (%).
These subjective assessments were in full agreement with the objective metrics: neither evaluation detected between-group differences in arterial image quality, while both confirmed significantly superior venous image quality in the experimental group.

Imaging Findings

The proposed dual-threshold tracking protocol successfully generated diagnostic-quality lower extremity vascular images in all participants. Figure 3 shows representative volume-rendered (VR) and curved planar reformation (CPR) images demonstrating patent and occluded arterial segments. Figure 4 demonstrates the post-surgical patency of a synthetic graft following aneurysm repair. Figure 5 presents a complex case of concurrent arteriovenous pathology, revealing venous thrombosis accompanied by secondary arterial compression.

Radiation Dose Assessment

No significant between-group differences were observed in radiation dose parameters (DLP and ED) between the two groups (all $P > 0.05$) (Table 4).

Table 4
Comparison of Radiation Dose Parameters Between the Two Groups

Phase	Parameter	Control Group	Experimental Group	*t*	*P*
Arterial Phase	DLP (mGy•cm)	720.48 ± 38.47	706.70 ± 35.72	1.531	0.131
	ED (mSv)	10.09 ± 0.54	9.89 ± 0.50	1.531	0.131
Venous Phase	DLP (mGy•cm)	402.68 ± 21.49	395.00 ± 18.21	1.591	0.117
	ED (mSv)	5.64 ± 0.30	5.53 ± 0.26	1.591	0.117

Note: Data are presented as mean ± standard deviation (SD). DLP = dose-length product. ED = effective dose.

Discussion

This study demonstrates that the dual-threshold bolus tracking technique, based on real-time monitoring of the distal abdominal aorta and popliteal vein, effectively compensates for individual hemodynamic variations and significantly improves venous phase image quality in one-stop lower extremity CTA-CTV. Our data indicate that, compared with traditional fixed-delay scanning, this individualized triggering strategy increased the proportion of diagnostic-quality venous images (score ≥ 3) from 55.9% to 88.2% ($P < 0.001$) without increasing the radiation dose. These findings further indicate that the dual-threshold technique effectively resolves the timing mismatch arising from inter-individual variations in circulation time, thereby offering a reliable one-stop solution for comprehensive lower extremity arteriovenous imaging while strictly adhering to the ALARA (As Low As Reasonably Achievable) principle.

Previous studies have highlighted the limitations of fixed-delay strategies used in conventional one-stop imaging, which are mainly attributed to significant inter-individual variations in circulation time (ranging from 15 to 45 seconds) [15, 23, 24]. Such population-averaged scan timing often fails to accommodate individual hemodynamic status, resulting in either insufficient venous filling or premature contrast washout [25, 26]. The high rate of non-diagnostic images (44.1%) observed in our control group is consistent with those reported by Asari et al. [27], further corroborating that the lack of individualized scan timing results in inconsistent image quality. To overcome these limitations, the dual-threshold protocol designed in this study utilizes the abdominal aorta as a stable initial trigger point and incorporates the popliteal vein as a real-time monitoring site that reflects lower extremity venous return. This design shifts the scan timing from a fixed, predetermined delay to a dynamic, physiologically driven adjustment, thereby enabling synchronization with the patient's circulatory timing and effectively mitigating the risk of imaging failure caused by inter-individual hemodynamic variation.

Preserving arterial phase quality while optimizing venous imaging was another critical focus of this study. Previous protocols that attempted to cover both arterial and venous phases with a single delay time often compromised peak arterial enhancement to permit venous filling, thereby decreasing proximal vessel attenuation [20, 28]. Nevertheless, our results did not demonstrate such a compromise. Li et al. [21]

suggested that 350 HU represents the optimal threshold for adequate vascular attenuation. In our study, the mean attenuation at the distal abdominal aorta (417.07 ± 98.79 HU) and popliteal artery (428.88 ± 108.58 HU) in the experimental group remained consistently above this threshold. These values not only exceed the minimum clinical requirements and align with the optimal thresholds reported by Nas et al. [16], but also indicate that our two-stage triggering approach successfully enabled sequential arteriovenous imaging. Crucially, the superior venous imaging was obtained without any sacrifice in arterial phase quality.

Furthermore, our results suggest that to achieve optimal vascular imaging, precise temporal control (i.e., optimal trigger timing) may be as critical as optimizing acquisition parameters. Chen et al. [29] reported a CNR of 7.06 by lowering the tube voltage to 70 kV, which takes advantage of the increased iodine attenuation at lower energy spectra. In contrast, at a relatively higher tube voltage of 80 kV, our study achieved a markedly higher popliteal vein CNR of 11.54 by tailoring the scan trigger to individual circulatory physiology with the dual-threshold technique. Although the imaging equipment and scanning parameters differed, this finding indicates that individualized scan timing driven by physiological feedback is as important a determinant of vascular CNR as acquisition parameter adjustments such as lowering tube voltage. This underscores that, when optimizing vascular imaging, physiology-driven timing control should not be regarded merely as an adjunct to acquisition parameters; it is an independent and powerful variable that can intrinsically improve CNR. A higher CNR signifies effective background noise suppression and vascular signal enhancement, directly yielding diagnostic benefits for the clinical identification of minute or mural thrombi.

While the current findings establish the clinical feasibility and image quality benefits of this protocol, its generalizability to broader populations—particularly those with complex hemodynamic conditions, significant vascular variants, or metallic implants—awaits prospective validation in larger multicenter cohorts. Moreover, as the present evaluation centered on image quality metrics, future studies incorporating DSA as a reference standard will be essential to fully define its diagnostic accuracy for thrombus detection.

Conclusions

By implementing a dual-threshold tracking technique, this study anchors the imaging trigger logic directly to the patient's real-time individual hemodynamics, thereby effectively resolving the challenge of inaccurate venous phase capture caused by inter-individual circulatory variations in one-stop combined lower extremity CTA-CTV. This technological advancement transitions the scanning paradigm from executing rigid, standardized protocols to dynamically accommodating individual physiological variations, ultimately providing a highly efficient and robust solution for combined lower extremity arteriovenous imaging in clinical practice.

Declarations

Ethics approval and consent to participate:

The study was conducted in accordance with the Declaration of Helsinki and approved by the Ethics Committee of the First Affiliated Hospital of Jinan University (Approval No. KY-2024-151). Written informed consent was obtained from all participants.

Consent for publication:

Not applicable. This manuscript contains no individual person's data.

Competing interests:

The authors declare no competing interests.

Funding:

No specific funding was received for this study.

Author Contribution

QPZ, SAG, YLX, TW, and ZH designed the study, collected the clinical and imaging data, and drafted the manuscript. QPZ and SAG performed the image quality assessments. YLX and TW conducted the statistical analysis. CZS conceptualized the research, supervised the project, and critically revised the manuscript for important intellectual content. All authors read and approved the final manuscript.

Acknowledgements:

Not applicable.

Data Availability

The datasets used and analyzed during the current study are available from the corresponding author on reasonable request. Individual de-identified imaging data are not publicly available due to hospital privacy regulations, but may be accessed with formal institutional permission.

References

1. Deng L, Du C, Liu L, Wang Y, Gu H, Armstrong DG et al. Forecasting the Global Burden of Peripheral Artery Disease from 2021 to 2050: A Population-Based Study. Research (Wash D C). 2025;8:0702.

2. Nehler MR, Duval S, Diao L, Annex BH, Hiatt WR, Rogers K, et al. Epidemiology of peripheral arterial disease and critical limb ischemia in an insured national population. J Vasc Surg. 2014;60:686–e695682.
3. Aday AW, Matsushita K. Epidemiology of Peripheral Artery Disease and Polyvascular Disease. Circ Res. 2021;128:1818–32.
4. Keller K, Prochaska JH, Coldewey M, Göbel S, Schmitt VH, Hahad O, et al. Atherosclerosis and Its Impact on the Outcomes of Patients with Deep Venous Thrombosis. Life (Basel). 2022;12:734.
5. Mandaglio-Collados D, Marín F, Rivera-Caravaca JM. Peripheral artery disease: Update on etiology, pathophysiology, diagnosis and treatment. Med Clin (Barc). 2023;161:344–50.
6. Criqui MH, Matsushita K, Aboyans V, Hess CN, Hicks CW, Kwan TW, et al. Lower Extremity Peripheral Artery Disease: Contemporary Epidemiology, Management Gaps, and Future Directions: A Scientific Statement From the American Heart Association. Circulation. 2021;144:e171–91.
7. Aboyans V, Ricco JB, Bartelink MEL, Björck M, Brodmann M, Cohnert T, et al. 2017 ESC Guidelines on the Diagnosis and Treatment of Peripheral Arterial Diseases, in collaboration with the European Society for Vascular Surgery (ESVS): Document covering atherosclerotic disease of extracranial carotid and vertebral, mesenteric, renal, upper and lower extremity arteries. Endorsed by: the European Stroke Organization (ESO) The Task Force for the Diagnosis and Treatment of Peripheral Arterial Diseases of the European Society of Cardiology (ESC) and of the European Society for Vascular Surgery (ESVS). Eur Heart J. 2018;39:763–816.
8. Sykora D, Firth C, Girardo M, Bhatt S, Tseng A, Chamberlain A, et al. Peripheral artery disease and the risk of venous thromboembolism. Vasa. 2022;51:365–71.
9. Shen S, Lan Y, He L, Li J, Li M, Chen Y. Non-contrast-enhanced magnetic resonance imaging technique diagnoses DVT and classifies thrombus. J Thromb Thrombolysis. 2022;53:663–70.
10. Uppot RN, Sahani DV, Hahn PF, Gervais D, Mueller PR. Impact of obesity on medical imaging and image-guided intervention. AJR Am J Roentgenol. 2007;188:433–40.
11. D'Oria M, Girardi L, Amgad A, Sherif M, Piffaretti G, Ruaro B, et al. Expert-Based Narrative Review on Compression UltraSonography (CUS) for Diagnosis and Follow-Up of Deep Venous Thrombosis (DVT). Diagnostics (Basel). 2025;15:82.
12. Neris R, Kimyaghalam A, Singh K. Comparison of Duplex Ultrasound and Digital Subtraction Angiography for Assessing Tibial Vessel Disease. Cureus. 2024;16:e69327.
13. Shetty AS, Hoegger MJ, Rajput MZ, Itani M, Nhan DT, Perez AA, et al. Aortoiliofemoral Lower Extremity CT Angiography Radiographics. 2025;45:e240272.
14. International Commission on Radiological Protection. The 2007 Recommendations of the International Commission on Radiological Protection. ICRP publication 103. Ann ICRP. 2007;37:1–332.
15. Tran TT, Kristiansen CH, Thomas O, Roy S, Haidl F, Ashraf H, et al. Indirect CT venography of the lower extremities: impact of scan delay and patient factors on contrast enhancement and examination quality. Eur Radiol. 2022;32:7946–55.

16. Nas L, Hoppe BF, Stüber AT, Grosu S, Fink N, von Fragstein A, et al. Optimizing lower extremity CT angiography: A prospective study of individualized vs. fixed post-trigger delays in bolus tracking. Eur J Radiol. 2025;185:112009.
17. Shi WY, Wang LW, Wang SJ, Yin XD, Gu JP. Combined Direct and Indirect CT Venography (Combined CTV) in Detecting Lower Extremity Deep Vein Thrombosis. Med (Baltim). 2016;95:e3010.
18. Williams BA, Doddamani S, Troup MA, Mowery AL, Kline CM, Gerringer JA, et al. Agreement between heart failure patients and providers in assessing New York Heart Association functional class. Heart Lung. 2017;46:293–9.
19. Tian Q, Zhu S, Cheng Y, Li J, Qu T, Jia X, et al. Improving image quality consistency and diagnostic accuracy in lower extremity CT angiography using a split-bolus contrast injection protocol. Br J Radiol. 2024;97:838–43.
20. Bae KT. Intravenous contrast medium administration and scan timing at CT: considerations and approaches. Radiology. 2010;256:32–61.
21. Li XS, Geng JG, Zhu YH, Liu LY, Qiao YQ, Ma YL, et al. CT imaging using variable helical pitch scanning for lower extremity arterial disease: Reduced contrast medium dose, improved image quality and diagnostic accuracy. Eur J Radiol. 2024;181:111792.
22. Christner JA, Kofler JM, McCollough CH. Estimating effective dose for CT using dose-length product compared with using organ doses: consequences of adopting International Commission on Radiological Protection publication 103 or dual-energy scanning. AJR Am J Roentgenol. 2010;194:881–9.
23. Zhou PL, Wu G, Han XW, Bi YH, Zhang WG, Wu ZY. Detection and characterization of Budd-Chiari syndrome with inferior vena cava obstruction: Comparison of fixed and flexible delayed scan time of computed tomography venography. Eur J Radiol. 2017;91:52–6.
24. Hinzpeter R, Eberhard M, Gutjahr R, Reeve K, Pfammatter T, Lachat M, et al. CT angiography of the aorta: contrast timing by using a fixed versus a patient-specific trigger delay. Radiology. 2019;291:531–8.
25. Chung JW, Yoon CJ, Jung SI, Kim HC, Lee W, Kim YI, et al. Acute iliofemoral deep vein thrombosis: evaluation of underlying anatomic abnormalities by spiral CT venography. J Vasc Interv Radiol. 2004;15:249–56.
26. Toh MR, Damodharan K, Lim H, Tang TY. Computed tomography venography versus intravascular ultrasound in the diagnosis of iliofemoral vein stenosis. Vasa. 2021;50:38–44.
27. Asari Y, Yasaka K, Kurashima J, Katayama A, Kurokawa M, Abe O. Deep learning reconstruction enhances image quality in contrast-enhanced CT venography for deep vein thrombosis. Emerg Radiol. 2025;32:699–708.
28. Iyama Y, Nakaura T, Kidoh M, Katahira K, Oda S, Utsunomiya D, et al. Relationships between patient characteristics and contrast agent dose for successful computed tomography venography with a body-weight-tailored contrast protocol. Med (Baltim). 2018;97:e0231.
29. Chen D, Zhou J, Wang P, Ge Q, Xu M, Qiu W, et al. Low-tube-voltage combined with adaptive statistical iterative reconstruction-V technique in CT venography of lower limb deep vein thrombosis. Sci Rep.

2018;8:11174.

Figures

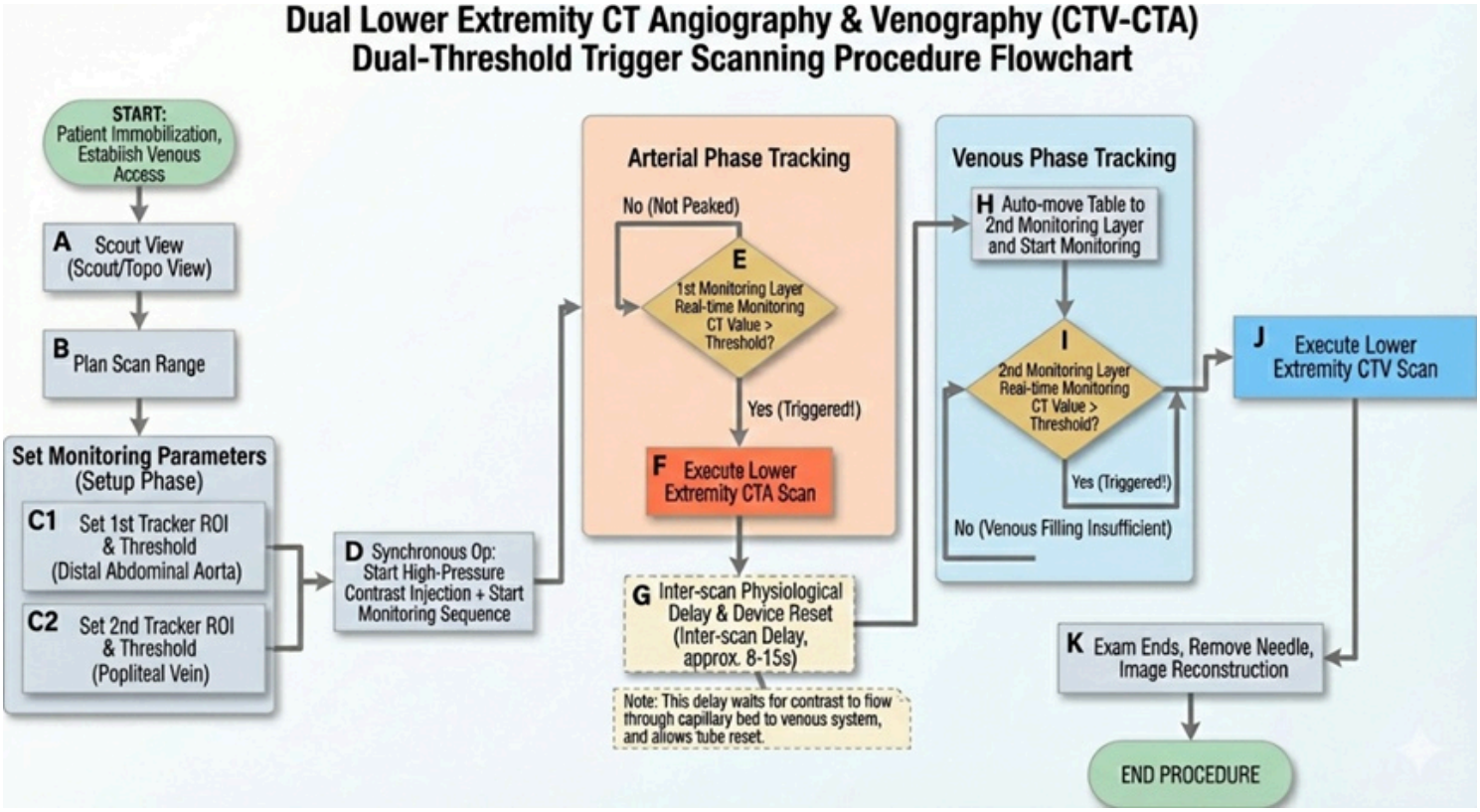


Figure 1

Dual-threshold bolus tracking protocol flowchart for one-stop lower extremity CTA-CTV.

The procedure initiates with a scout view and planning phase. During the setup phase, two monitoring regions of interest (ROIs) are placed at the distal abdominal aorta (150 HU threshold) and the popliteal vein (120 HU threshold). The scan involves a sequential trigger logic: (a) arterial phase tracking triggers the CTA scan; (b) an inter-scan delay allows for physiological transit and table movement; (c) venous phase tracking triggers the CTV scan. This workflow ensures individualized synchronization with the patient's hemodynamic status.

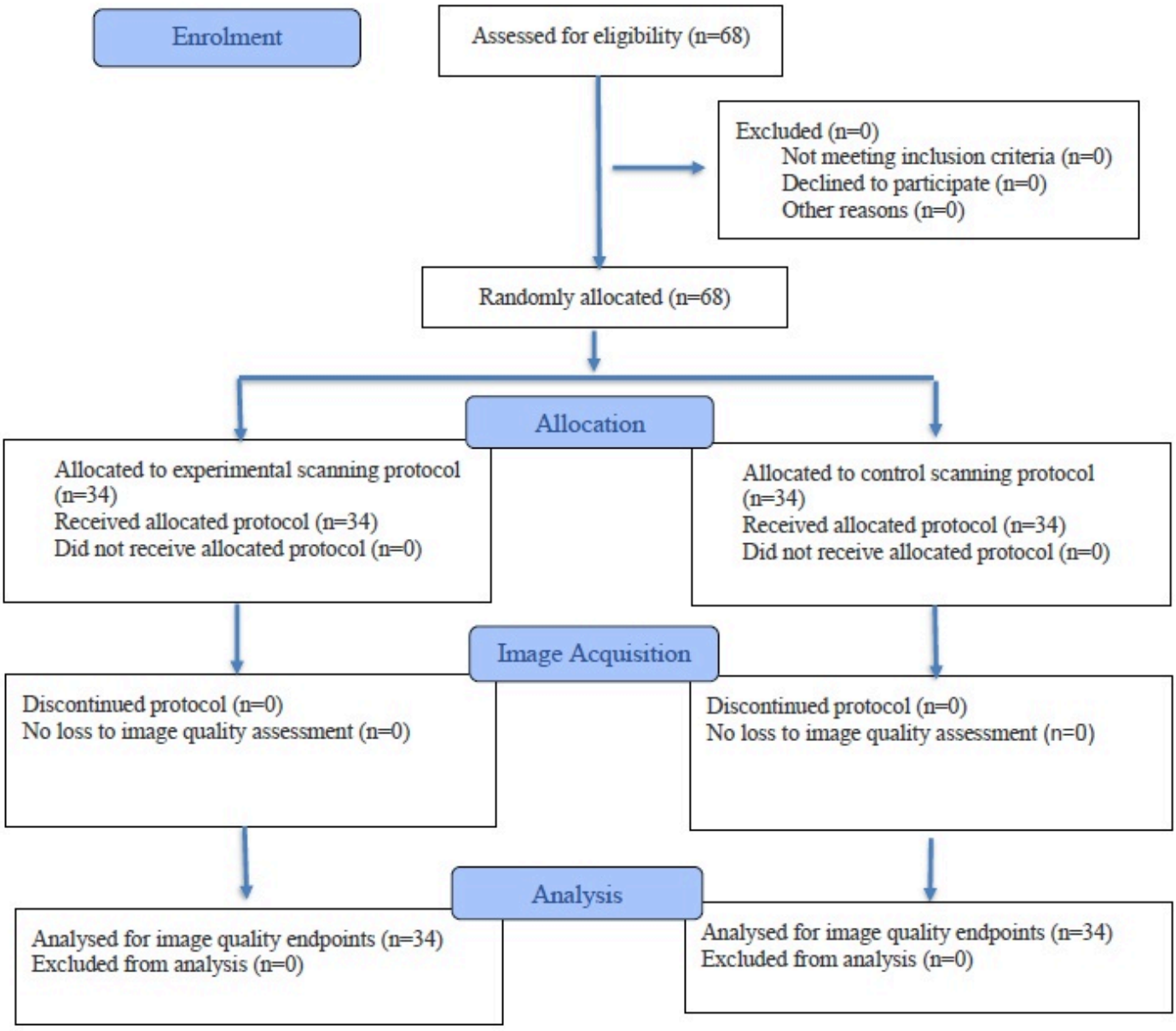


Figure 2

Flow diagram of patient allocation in the comparative imaging protocol assessment.

A total of 68 patients with suspected lower extremity vascular disease were assessed for eligibility and randomly allocated to either the experimental group (dual-threshold bolus tracking, n=34) or the control group (fixed 165-second delay, n=34). All participants received their allocated scan protocol, with no losses to follow-up or exclusions from the final image quality analysis.

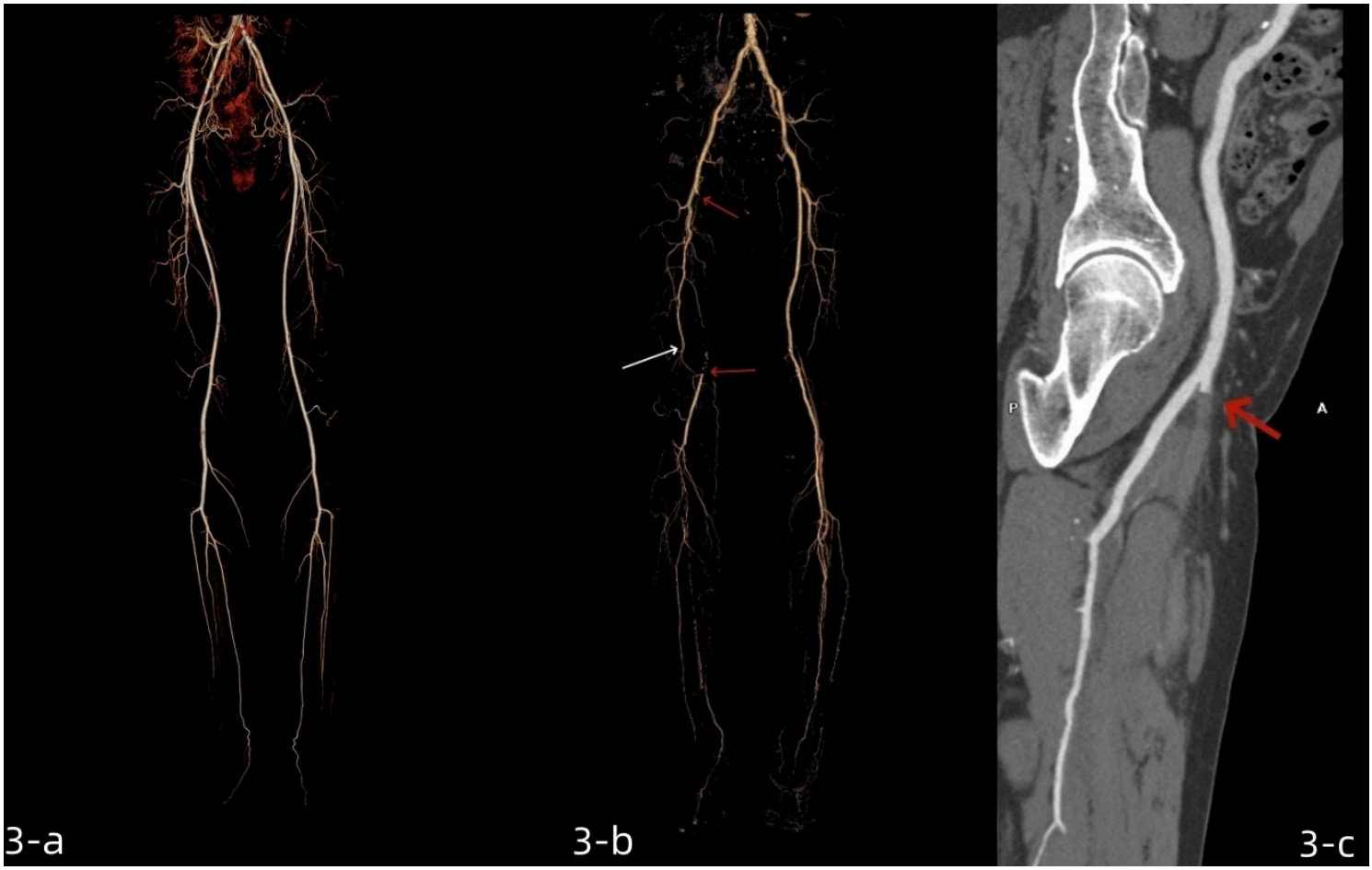


Figure 3

Representative CTA images of lower extremity arterial patency and occlusion.

(3-a) Bone-subtracted volume-rendered (VR) CTA image of a 31-year-old female, displaying the entire lower extremity arterial tree with natural vessel coursing and no significant stenosis or occlusion. (3-b) Bone-subtracted VR CTA image of a 75-year-old male, revealing complete occlusion of the mid-segment of the right femoral artery (red arrow) with the formation of compensatory collateral circulation (white arrow). (3-c) Curved planar reformation (CPR) image of the same patient in (3-b), clearly delineating the proximal origin of the right femoral artery occlusion (red arrow), with the occluded segment extending approximately 3.2 cm.

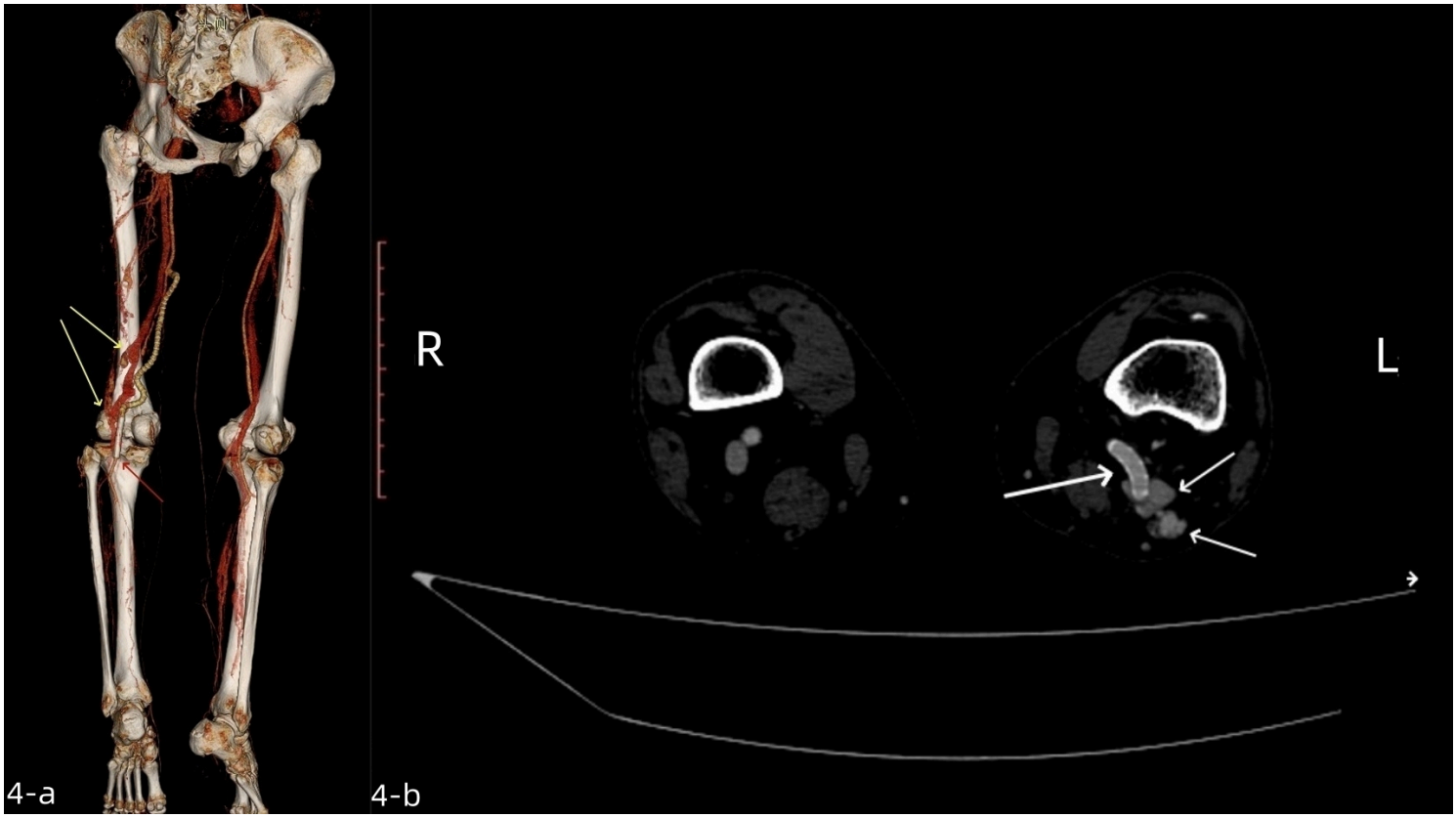


Figure 4

Combined lower extremity arteriovenous imaging in a patient during post-aneurysm surgery follow-up.

(4-a) VR CTA image (with bone) showing the aneurysm sac measuring approximately 55 mm × 42 mm (yellow arrows). The end-to-side anastomosis between the synthetic graft and the proximal popliteal artery is patent (red arrow). (4-b) Axial image demonstrating the anatomical relationship between the synthetic graft and the accompanying vein (white arrows), with no evidence of abnormal arteriovenous communication.

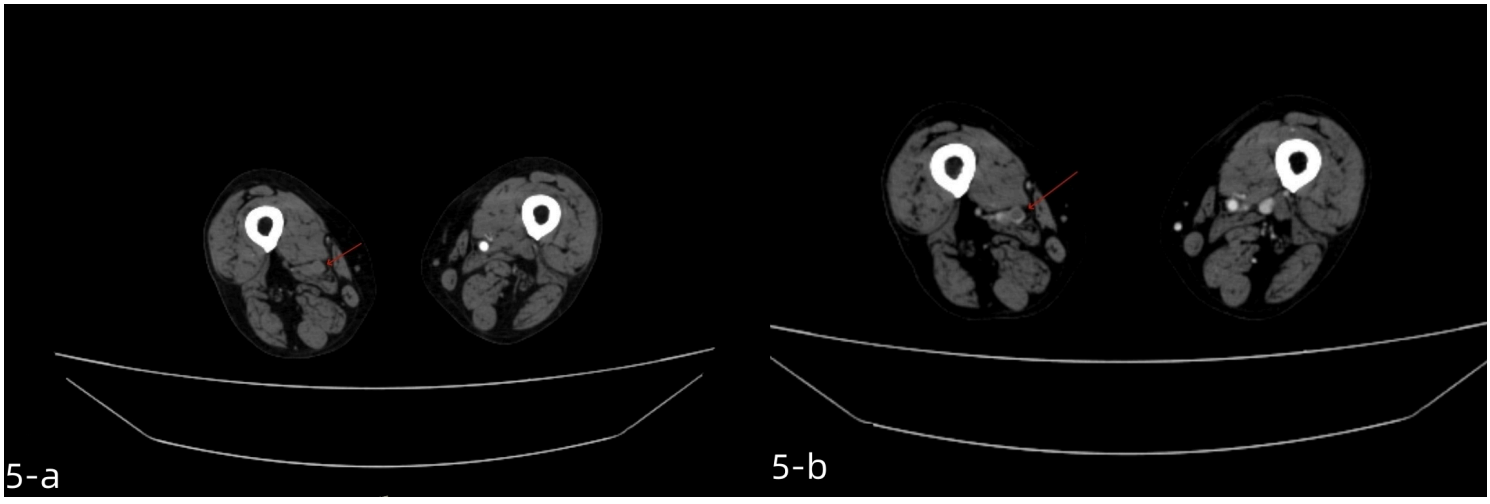


Figure 5

Combined lower extremity arteriovenous imaging in a patient with concurrent arterial and venous pathology.

(5-a) Arterial phase axial image showing complete luminal occlusion of the right femoral artery (red arrow). (5-b) Venous phase axial image revealing a filling defect within the ipsilateral femoral vein (red arrow), suggesting thrombosis with secondary compression and occlusion of the adjacent artery.

Supplementary Files

This is a list of supplementary files associated with this preprint. Click to download.

- Figure1.jpg
- Figure2.jpg
- Figure3.jpg
- Figure4.jpg
- Figure5.jpg
- Additionalfile1.docx